Progress In Electromagnetics Research C, Vol. 104, 69–84, 2020

Transient Response of Microstrip Patch Antenna Loaded on a Vehicle Platform Illuminated by Electromagnetic Pulse

Xiao Hu*, Yang Qiu, Qinglin Xu, and Jin Tian

Abstract—This paper presents an efficient hybrid method consisting of nonuniform mesh finite-difference-time-domain (FDTD) method, thin wire model, and transmission line (TL) equations method, which is utilized to analyze transient responses of the microstrip patch antenna loaded on a vehicle platform illuminated by a high-power electromagnetic pulse (EMP). This hybrid method avoids over-fine mesh generation, thereby improving the computational efficiency and saving the computational memory. The accuracy and efficiency of this method are verified by comparing with the simulation results of traditional FDTD and computer simulation technology microwave studio (CST MWS). Then, considering the influence of the incident conditions of EMP and the support structure of antenna on the coupling effects of the antenna, the coupling responses of the 1.575 GHz microstrip antenna are discussed in terms of incident angles of EMP, heights of the support structure, top areas of the support structure, and different positions of the support structure on the platform. The obtained changing regularity of the transient responses is useful for further designing the installation structure of the antenna and electromagnetic protection against the external EMP.

1. INTRODUCTION

In recent years, with the rapid development of high-power electromagnetic pulse (EMP) source, electronic devices are confronted with new and rigorous challenges. The pulse interference signal has the characteristics of short rising time and large pulse amplitude, which may cause electromagnetic interference or even damage to electronic equipment. Therefore, the coupling effect of high-power EMP to electronic equipment has become a research hotspot [1–4]. Microstrip patch antennas are widely used in communication and navigation equipment of vehicle, aircraft, missile and other system platforms because of their advantages of light weight, small size, thin profile, etc. However, due to its fragile protective performance, the microstrip patch antenna in navigation equipment are susceptible to electromagnetic interference, especially when it is illuminated by EMP. Hence, it is necessary to investigate the coupling effects of EMP to microstrip patch antenna.

The coupling path of EMP to electronic system can be divided into front-door coupling and back-door coupling. Front-door coupling mainly refers to the effect that the EMP enters into the receiver through the antenna of the system. Back-door coupling is relatively complex, including some slots, apertures, windows, and interconnected cables in the metallic enclosure. In the published papers, many researches focus on the back-door coupling effect of EMP on electronic systems, and the preferred method used to simulate the coupling problem is the full-wave algorithm. For example, Lertsirimit et al. [5] used a combination of transmission-line analysis and full-wave solver to calculate the coupling to a printed circuit board inside a cavity by a wire penetrating an aperture. Xie et al. [6–8] established the SPICE (Simulation program with integrated circuit emphasis) models of different transmission lines to calculate the transient response of EMP on the cable based on the finite-difference time domain

Received 23 December 2019, Accepted 5 March 2020, Scheduled 24 July 2020
* Corresponding author: Xiao Hu (wohuxiao123@163.com).
The authors are with the Electromagnetic Compatibility Laboratory, Xidian University, Xi'an 710071, China.

(FDTD)-SPICE hybrid method. Ye et al. [9–11] proposed FDTD-TL (transmission line) method to analyze the electromagnetic interference (EMI) coupling of EMP to transmission lines termination in different scenarios.

It should be noted that in the actual electromagnetic environment, the electromagnetic energy entering the target through the back-door coupling is very limited, and most of the energy is mainly coupled into the target through the antenna. However, there are not many research works concerning the coupling between EMP and antenna. In [12–15], the transient response in the time domain (TD) of monopole or dipole antenna illuminated by EMP is captured with different methods. Taking the influence of other factors in the system into account, the system TD response of a metallic enclosure with thin-wire antenna and transmission line is predicted based on hybrid FDTD method in [16–19]. However, these studies are only aimed at simple thin wire antennas. The behavior of a microstrip patch antenna fed with a wire (coaxial probe) and illuminated by an electromagnetic pulse is analyzed by using a total finite difference algorithm [20], in which the numerical Huygen's source scheme is used to illuminate the antenna, and the Thevenin equivalent circuits are established. However, the method needed complicated formula derivation and the analysis did not consider the scene when the antenna is installed on the platform.

In this paper, we present a time-domain hybrid method for investigating the coupling effects of high power EMP to the microstrip patch antenna. In order to rapidly capture the time domain response of the microstrip patch antenna, the hybrid method combines the non-uniform mesh FDTD, thin-wire model and the transmission line equations method effectively. Especially, considering the influence of an installing platform on the coupling effects of the microstrip patch antenna, the coupling characteristics of the antenna installed on a simplified vehicle platform are discussed in detail in terms of the incident angles of EMP, the heights of the support structure, the top areas of support structure, and different positions of support structure on the platform.

2. THEORY OF THE HYBRID METHOD

The model of a typical square microstrip antenna is shown in Fig. 1, which is comprised of a radiation patch, an FR4 (epoxy glass fiberboard) dielectric substrate, and a perfect conducting ground plane. The relative dielectric constant of the substrate is ε_r. The antenna fed by a coaxial cable is mounted on a cylindrical support structure on a vehicle platform of dimensions $L_1 \times L_2 \times L_3$, which is illuminated by an external EMP, as shown in Fig. 2.

In order to analyze the time domain response of the microstrip patch antenna on the vehicle platform, in ordinary circumstances, the whole problem space would be meshed uniformly. However, since the size of microstrip antenna containing coaxial feed probe is much smaller than that of vehicle platform, and the electromagnetic field around the discontinuous structure of antenna vary dramatically,

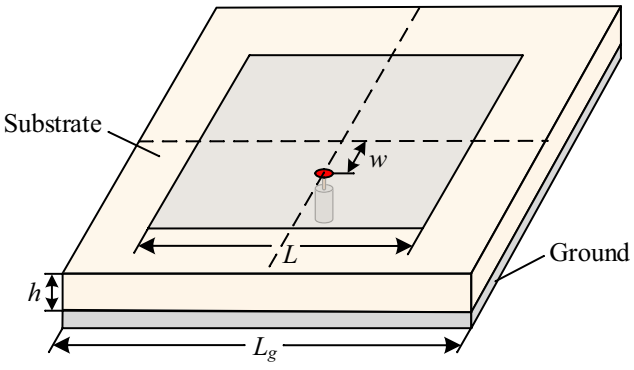

Figure 1. Geometry of a square microstrip patch antenna.

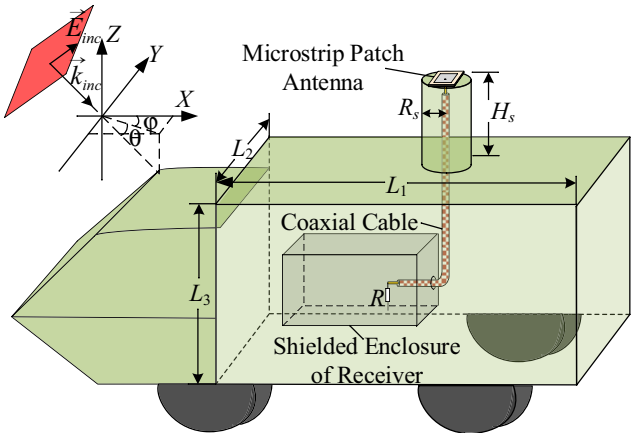

Figure 2. Geometry of the microstrip patch antenna installed on a simplified vehicle platform.

it needs finer mesh size for modeling the antenna to achieve the expected simulation accuracy. Thus, the non-uniform mesh [21] FDTD scheme is utilized to solve the simulation domain rather than using smaller mesh alone uniformly throughout the space domain, thereby increasing the computation efficiency. Then, we incorporate the modified thin-wire model and transmission-line feeding model into the FDTD scheme, so as to avoid extremely fine meshing when modeling the coaxial feeding port. The detailed formulation of this hybrid method will be given in the following sections.

2.1. Nonuniform Mesh FDTD Method

The time-dependent Maxwell's curl equations for linear, isotropic, non-dispersive and lossless media are written as

$$\nabla \times \mathbf{H} = \varepsilon \frac{\partial \mathbf{E}}{\partial t} \tag{1}$$

$$\nabla \times \mathbf{E} = -\mu \frac{\partial \mathbf{H}}{\partial t} \tag{2}$$

where $\mathbf{E}$ and $\mathbf{H}$ are the electric and magnetic vector fields, respectively. ε is the permittivity, and μ is the permeability of the medium. According to the conventional FDTD method based on Yee's grid, Equations (1) and (2) can be solved, then the updating equations of the E_z and H_z components can be given by

$$\begin{aligned} E_z^{n+1}(i,j,k) &= E_z^n(i,j,k) + \frac{\Delta t}{\varepsilon(i,j,k)} \\ &\quad \times \left[\frac{H_y^{n+\frac{1}{2}}(i,j,k) - H_y^{n+\frac{1}{2}}(i-1,j,k)}{\Delta x_i} - \frac{H_x^{n+\frac{1}{2}}(i,j,k) - H_x^{n+\frac{1}{2}}(i,j-1,k)}{\Delta y_j} \right] \end{aligned} \tag{3}$$

$$\begin{aligned} H_z^{n+\frac{1}{2}}(i,j,k) &= H_z^{n-\frac{1}{2}}(i,j,k) + \frac{\Delta t}{\mu(i,j,k)} \\ &\quad \times \left[\frac{E_x^n(i,j+1,k) - E_x^n(i,j,k)}{\Delta y_j} - \frac{E_y^n(i+1,j,k) - E_y^n(i,j,k)}{\Delta x_i} \right] \end{aligned} \tag{4}$$

Here, i, j, k and n are the space and time indexes. Δt is the time step, and Δx_i, Δy_j, Δz_k, are the space increments along the x-, y-, and z-directions, respectively. The other field components E_x, E_y, H_x and H_y have the similar expressions. In the classic formulation of the FDTD method, since the computational domain and the time axis are uniformly discretized, it requires a lot of computational cost when the mesh size is very small. Therefore, in our hybrid method, the problem space is divided into fine mesh domain and coarse mesh domain.

As shown in Fig. 3, the fine mesh is applied to divide the antenna and its near region, and the coarse one is applied to divide the other space between antenna and the absorbing boundary. Δx_f, Δy_f, Δz_f are the space increments of fine mesh domain along the x-, y-, and z-directions, respectively. Δx_c, Δy_c, Δz_c are the space increments of coarse domain, respectively. By using the non-uniform mesh FDTD, the field values in the coarse mesh region, fine mesh region as well as on the boundaries can be updated simultaneously, where the difference is that in a fine mesh region, the space increments Δx_i, Δy_j, Δz_k of Equations (3) and (4) are equal to Δx_f, Δy_f, Δz_f respectively; and in the coarse region, the space increments are equal to Δx_c, Δy_c, Δz_c respectively.

It should be noted that, when solving the electric fields at the junction of coarse and fine mesh, in order to reduce the reflection error from fine-coarse boundary because of the discontinuity, the linear interpolation [22] on the coarse-fine boundary in space is applied in our method. Based on linear interpolation from $H_y(i-1,j,k)$ and $H_y(i,j,k)$ components, an assumed magnetic field component $H'_y(i,j,k)$ at a distance of half fine mesh interval from coarse-fine boundary is given by

$$H'_y(i,j,k) = \frac{p-1}{p+1} H_y(i-1,j,k) + \frac{2}{p+1} H_y(i,j,k) \tag{5}$$

where $p = \Delta_{\text{coarse}}/\Delta_{\text{fine}}$ is the ratio of two kinds of mesh sizes. The other directions have the similar expressions.

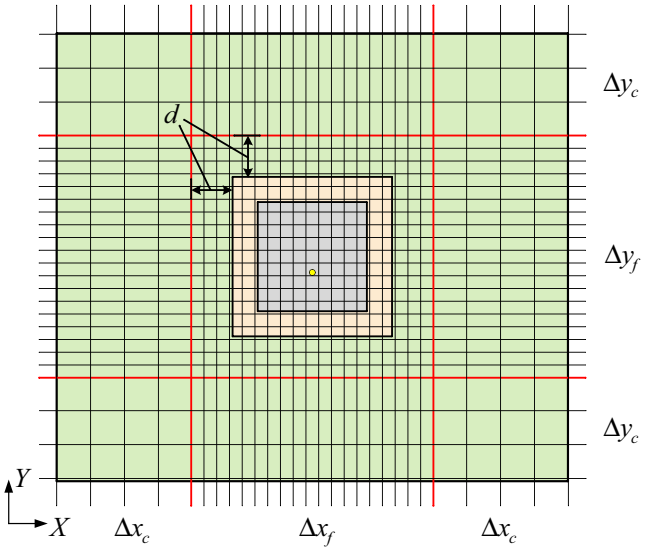

Figure 3. The model of non-uniform mesh generation.

The space increments at the coarse-fine boundary need to take the average value of two different mesh sizes, as shown in Fig. 4(a), where the space increments of electric fields updating equation along three directions are given by

$$\begin{aligned} \Delta x_i &= (\Delta x_f + \Delta x_c)/2 \\ \Delta y_i &= (\Delta y_f + \Delta y_c)/2 \\ \Delta z_i &= (\Delta z_f + \Delta z_c)/2 \end{aligned} \tag{6}$$

For the magnetic field at the junction, since the magnetic field is at the center of the mesh, as shown in Fig. 4(b), the space increments of magnetic fields updating equation do not require special treatment.

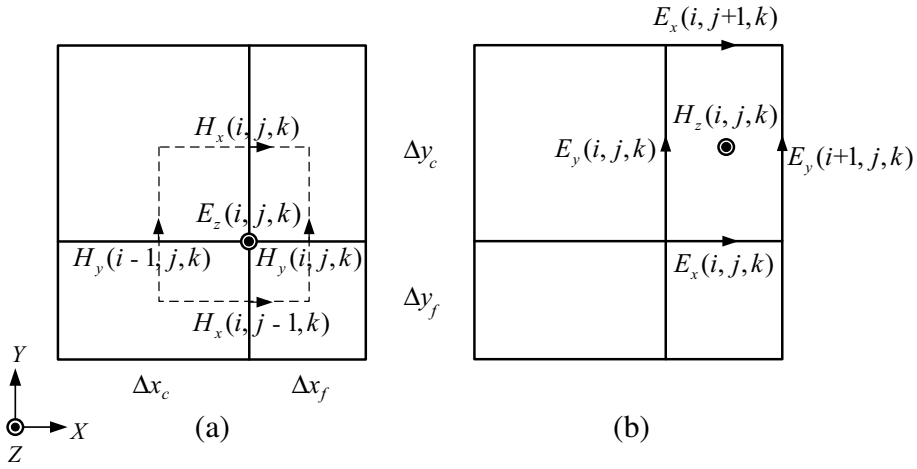

Figure 4. The fields at the junction of coarse and fine mesh. (a) The magnetic fields around the E_z; (b) The electric fields around the H_z.

2.2. Coaxial Feed Model

Since the size of coaxial line is usually less than one mesh size, as shown in Fig. 5, there are some coaxial feeding models available in FDTD. In these models, the feed probe connected to the coaxial feed line

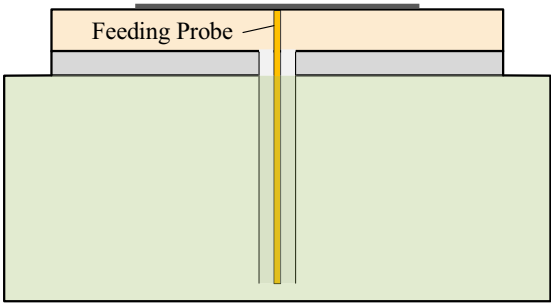

Figure 5. The configuration of coaxial feeding model.

is simulated by a simple wire model, and the propagation of electromagnetic field inside a coaxial feed line is simulated by a 1-D transmission line model. The thin wire representation of coaxial feed probe has great influence on the simulation accuracy. Therefore, for the improved thin wire representation of feed probe, we have several choices to simulate in FDTD domain. Umashankar et al. [27], Noda and Yokoyama [28], MäKinen et al. [29], and Railton et al. [30, 31] have proposed thin wire representations for FDTD computations in the three-dimensional (3D) Cartesian coordinate system.

However, for a conductor system having a radius, a, smaller than $0.15\Delta r$ or larger than $0.65\Delta r$ (Δr is the lateral side length of mesh used), when being modeled using the thin wire representations of Noda and Yokoyama, and Railton et al., with a time increment determined from the upper limit of Courant stability condition (about $0.99\Delta r/c/\sqrt{3}$, where c is the speed of light), it will result in numerical instability. Therefore, based on the previous research, Taniguchi et al. [32] have proposed an improved representation of an arbitrary-radius wire which enables FDTD computations to be carried out stably and accurately. Thus, we extend Taniguchi's model to be applicable for our hybrid method to get a high efficiency as well as a low computational cost. Note that, since this paper mainly analyzes the coupling response of antenna, the thin wire probe and coaxial line are assumed to be lossless. Based on the Noda's model [28], the relative permeability used for calculating the magnetic field components closest to the wire, and the relative permittivity used for getting the closest radial electric field components can be given by

$$\begin{aligned} \mu_r' &= \frac{\mu_r}{m}, \quad \varepsilon_r' = m\varepsilon \\ m &= \frac{\ln\left(\dfrac{\Delta r}{a_0}\right)}{\ln\left(\dfrac{\Delta r}{a}\right)}, \quad a_0 = 0.23\Delta r \end{aligned} \tag{7}$$

where $\Delta r = \Delta x_f = \Delta y_f = \Delta z_f$ is the space increments of fine mesh region; μ_r and ε_r are the relative permeability and permittivity of the original medium surrounding the wire; a_0 is the equivalent radius; and a is the actual radius of thin wire.

In order to avoid the numerical instability, when the radius of a z-directed thin wire, a, is smaller than the equivalent radius, a_0, in addition to the closest circulating magnetic field components, H_x and H_y, the modified relative permeability, μ_r', given by Eq. (7), should be employed in calculating the axial magnetic field components closest to the wire, H_z, as shown in Fig. 6(a). Similarly, when the radius of a z-directed thin wire, a, is larger than the equivalent radius, a_0, in addition to the closest radial electric field components, E_x and E_y, the modified relative permeability, ε_r', should be employed in calculating the axial electric field components closest to the wire, E_z, as shown in Fig. 6(b).

For the coaxial feed model of antenna, the behavior of the internal electromagnetic field of the coaxial line is solved by applying transmission line theory, as shown in Fig. 7. The transmission-line equations can be discretized by one-dimensional (1-D) FDTD scheme, which are given by

$$I^{n+1/2}(k') = I^{n-1/2}(k') - \frac{c\Delta t}{Z_a \Delta z}\left[U^n(k'+1) - U^n(k')\right] \tag{8}$$

$$U^{n+1}(k') = U^n(k') - Z_a \frac{c\Delta t}{\Delta z}\left[I^{n+1/2}(k'+1) - I^{n+1/2}(k')\right] \tag{9}$$

where U and I represent the voltage and current vector of the coaxial cable, respectively. k' is the

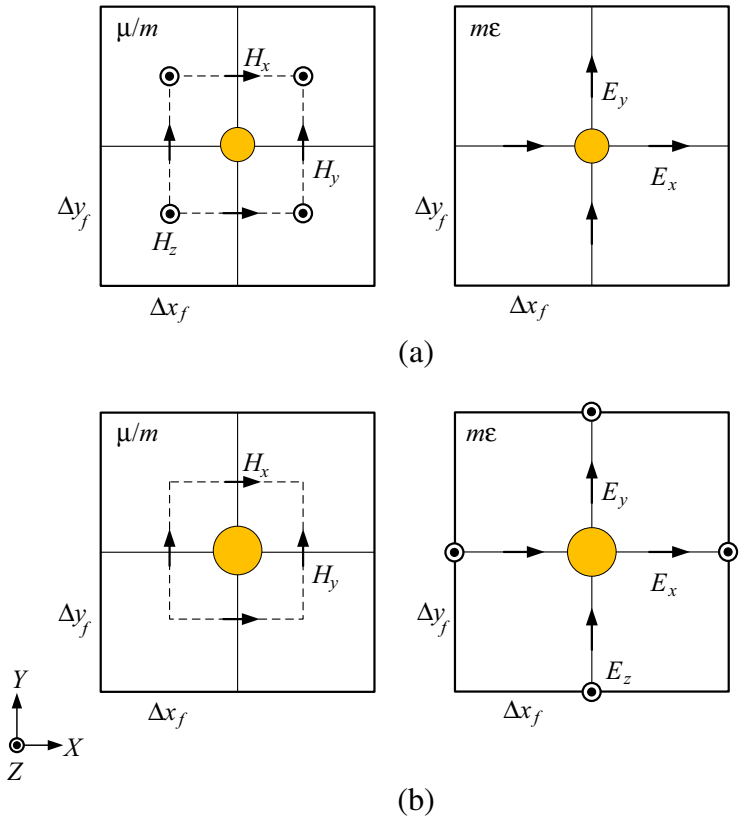

Figure 6. The configuration of coaxial feeding model. (a) $a < a_0$, (b) $a > a_0$.

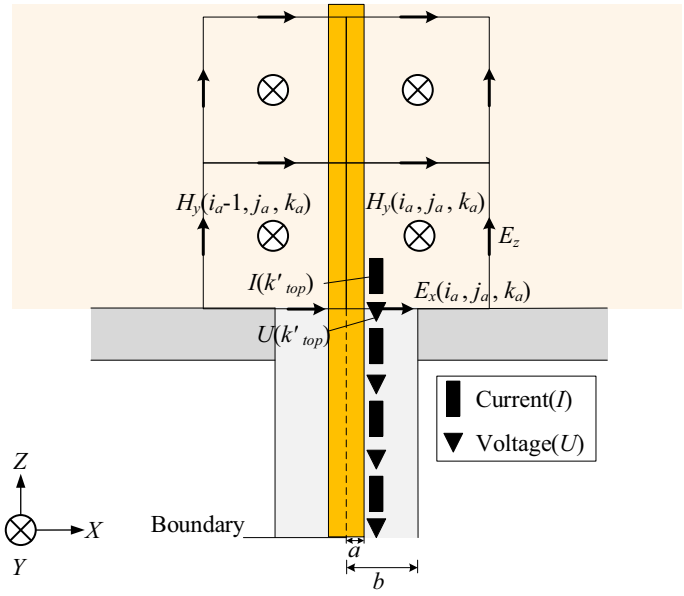

Figure 7. The configuration of coaxial feed model.

special index of the cable in the z-direction. Z_a is the characteristic impedance of coaxial cable. When the antenna is illuminated by an EMP, according to the Ampere's law, the current at the feeding point between coaxial cable and antenna can be calculated by

$$\begin{aligned} I^{n+1/2}(k'_{\text{top}}) &= \Delta y_f \left[H_y^{n+1/2}(i_a, j_a, k_a) - H_y^{n+1/2}(i_a - 1, j_a, k_a)\right] \\ &\quad -\Delta x_f \left[H_x^{n+1/2}(i_a, j_a, k_a) - H_x^{n+1/2}(i_a, j_a - 1, k_a)\right] \end{aligned} \tag{10}$$

where i_a, j_a, and k_a are the location indexes of the feeding mesh in the x-, y-, and z-directions, respectively. k'_{top} represents the feeding point of the cable.

Substituting Eq. (10) into Eqs. (8) and (9), the transient response of external electromagnetic interference coupled to cable through antenna can be obtained. Further, taking the effect of coaxial cable on the external field at the aperture into account, the equations for the magnetic field components surrounding the feeding point can be given by

$$\begin{aligned} H_y^{n+1/2}(i_a, j_a, k_a) &= H_y^{n-1/2}(i_a, j_a, k_a) - \frac{\Delta t}{\mu' \Delta z_f}\left[E_x^n(i_a, j_a, k_a + 1) - \frac{U^n\left(k'_{\text{top}}\right)}{b}\right] \\ &\quad + \frac{\Delta t}{\mu' \Delta x_f} E_z^n(i_a + 1, j_a, k_a) \end{aligned} \tag{11}$$

$$\begin{aligned} H_x^{n+1/2}(i_a, j_a, k_a) &= H_x^{n-1/2}(i_a, j_a, k_a) - \frac{\Delta t}{\mu' \Delta z_f}\left[E_y^n(i_a, j_a, k_a + 1) - \frac{U^n\left(k'_{\text{top}}\right)}{b}\right] \\ &\quad + \frac{\Delta t}{\mu' \Delta y_f} E_z^n(i_a, j_a + 1, k_a) \end{aligned} \tag{12}$$

where $U^n(k'_{\text{top}})$ is the voltage at the aperture, and it can be obtained by Equation (9). The updating equations of $H_y^{n+1/2}(i_a - 1, j_a, k_a)$ and $H_x^{n+1/2}(i_a, j_a - 1, k_a)$ can be modified in the same way.

3. NUMERICAL SIMULATION AND ANALYSIS

In this section, firstly, this hybrid method, traditional FDTD and the CST MWS [based on a finite integration technique (FIT)] are used to simulate a case, and the simulation results are compared to verify the accuracy and efficiency of the proposed method. Then, the coupling responses of the microstrip patch antenna mounted on the vehicle platform are discussed in detail in terms of the pitch angle of incident EMP, the azimuth angle of incident EMP, the heights of the support structure, the top areas of support structure, and different positions of support structure on the vehicle.

3.1. Verification of the Hybrid Method

The simulation case adopted is shown in Fig. 8, where the vehicle platform is simplified as a PEC enclosure with the dimension of $L_1 \times L_2 \times L_3 = 0.5\,\text{m} \times 0.5\,\text{m} \times 0.2\,\text{m}$ to save simulation time and

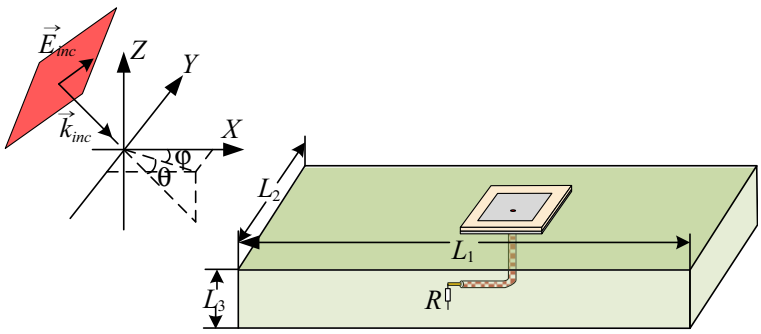

Figure 8. The model of antenna on a simplified PEC enclosure.

computational cost. We model a square microstrip antenna of patch length $L = 30\,\text{mm}$ over an infinite ground of length $L_g = 48\,\text{mm}$, with the substrate of thickness $h = 2\,\text{mm}$ and constant $\varepsilon_r = 9.5$ to satisfy the resonant frequency $f = 1.575\,\text{GHz}$. The antenna is placed at the center of the vehicle, which is fed by the coaxial cable, and its inner radius a and outer radius b are 0.25 mm and 0.58 mm, respectively, with its characteristic impedance set to $50\,\Omega$, and the terminal load R of the cable is $50\,\Omega$. The feed point deviates from antenna center $w = 3\,\text{mm}$ on Y axis.

The coarse mesh size and fine mesh size of nonuniform FDTD are chosen to be $\Delta x_f = \Delta y_f = \Delta z_f = 0.5\,\text{mm}$, $\Delta x_c = \Delta y_c = \Delta z_c = 5\,\text{mm}$, respectively, and the time step is chosen to be $\Delta t = 0.9\Delta x_f/\sqrt{3}c$ to satisfy the CFL (Courant Friedrichs Lewy) condition. The fine mesh area is set as a cuboid area $d = 20\,\text{mm}$ away from each side of the antenna in x, y, and z directions, as shown in Fig. 3. In our FDTD simulation, convolutional perfectly matched layer (CPML) [33] is used as the boundary condition in the solving domain. The incident directions of the EMP can be described by pitch angle θ, azimuth angle φ, and wave vector k_{inc}, as shown in Fig. 8. The polarization of E_{inc} is set to be parallel to the XOY plane and along y-direction, and the incident EMP wave is set in the directions of $\theta = 45^\circ$ and $\varphi = 0^\circ$, respectively. The excitation signal of the E_{inc} used in this example is described by a cosine modulated Gaussian pulse function as follows

$$E_{inc}(t) = E_0 \cos\left[2\pi f_0(t - t_0)\right] e^{-\left(\frac{t-t_0}{\tau}\right)^2} \tag{13}$$

where $E_0 = 30000\,\text{V/m}$, $f_0 = 1.575\,\text{GHz}$, $\tau = 2\,\text{ns}$, and $t_0 = 2.5\tau$. The time domain waveform is shown in Fig. 9. Then, the terminal responses of the microstrip antenna calculated by traditional FDTD (uniform mesh), CST MWS, and proposed method are compared, which is shown in Fig. 10. The detailed variations of time domain and frequency domain are in good agreement, and the main difference is time delay between the FDTD and CST MWS. That is because CST MWS is based on FIT, while our method is based on FDTD; their simulation calculation will lead to differences due to different types of the mesh generation of simulation. Therefore, the agreement between the results of proposed method and CST software is satisfactory.

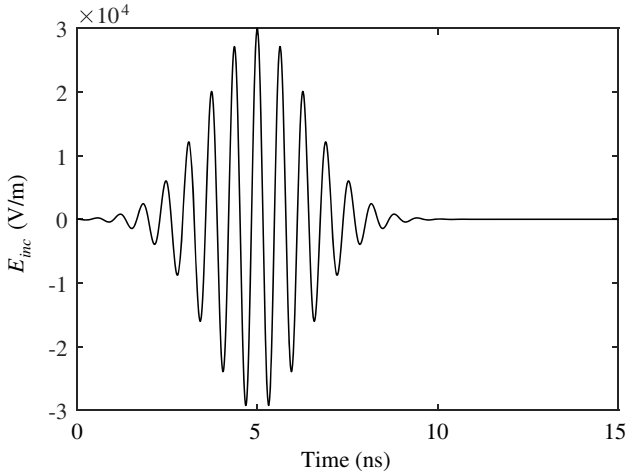

Figure 9. The time domain waveform of the incident EMP wave.

Table 1 shows the parameters of the mesh size, memory, simulation time, and CPU utilization in this case by three methods. All simulations and calculations are performed on the same workstation, which has 2 CPU with 16 cores (2.2 GHz) and 128 GB RAM. As the CST adopts parallel computing and memory optimization and consumes a lot of CPU (99%), its simulation speed is the fastest. However, compared with traditional FDTD, it is obvious that the time and memory needed by the hybrid method are much less than that for using the traditional FDTD method with uniform mesh only. Moreover, under the condition of low CPU utilization (38%), the simulation cost of our method is also satisfactory compared with CST.

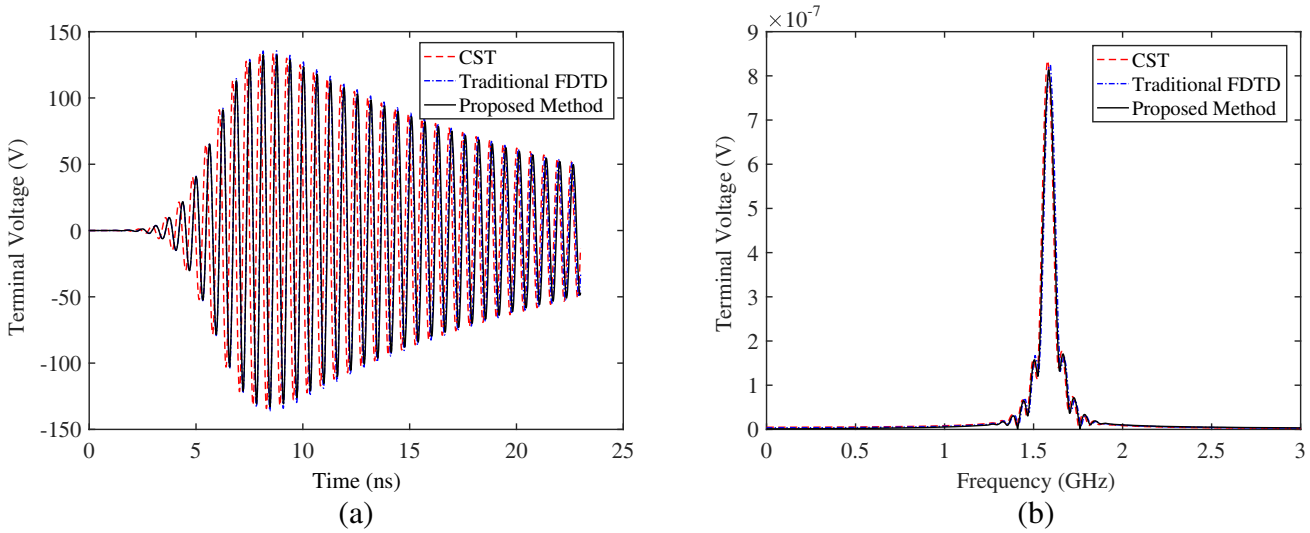

Figure 10. Comparison of the terminal voltage simulated by CST, traditional FDTD and proposed method (a) in time domain; and (b) in frequency domain.

Table 1. Simulation resource cost by three methods.

Method	Mesh Size	Memory	Simulation Time	CPU Utilization
CST MWS	Adaptive Mesh (minimum 0.5 mm)	1.69 GB	35 min	99%
Traditional FDTD	0.5 mm	89.87 GB	110 h 40 min	37%
Proposed Method	fine 0.5 mm and coarse 5 mm	3.64 GB	1 h 46 min	38%

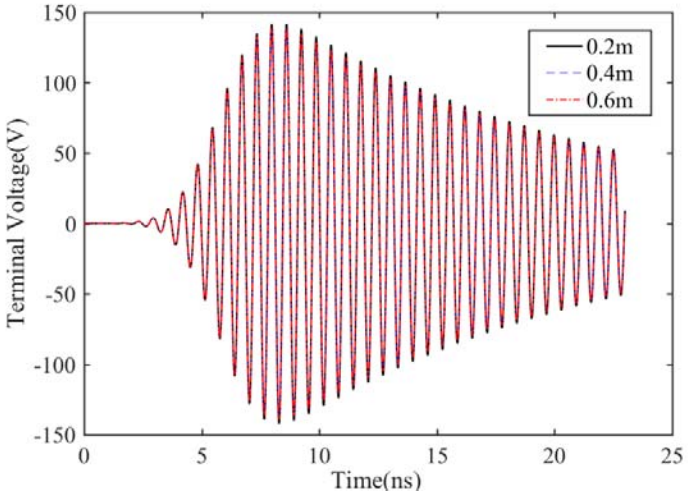

Figure 11. Terminal voltages at different vehicle heights L_3.

It should be noted that because we mainly consider the influence of vehicle top environment on the response of microstrip antenna, and the different height has little effect on the simulation results of microstrip antenna, as shown in Fig. 11, we set the height $L_3 = 0.2$ m in the subsequent simulation

analysis so as to save simulation time and computational cost. Furthermore, because the microstrip antenna is horizontally polarized, when the polarization of the E_{inc} of incident EMP is also horizontal, the polarizations of them are matched so that the electromagnetic signal received by the antenna will reach its maximum value. Therefore, the E_{inc} of the incident EMP is set to be parallel to the xoy plane in the subsequent sections.

3.2. Coupling Responses Considering Different Pitch Angle of Incident EMP

Next, the proposed method is firstly used to analyze the coupling response of antenna mounted on a support structure at different pitch angles θ. As shown in Fig. 12, the antenna is supported by a cylinder structure with the height of $H_s = 0.1\,\text{m}$ and the radius of $R_s = 20\,\text{mm}$ installed on the vehicle platform of dimensions $L_1 \times L_2 \times L_3 = 3\,\text{m} \times 2\,\text{m} \times 0.2\,\text{m}$. It is placed at the center of the top of the vehicle. The incident EMP wave is set in the direction of $\varphi = 0°$, and θ varies from 0° to 180° by 15° increments. When the EMP is incident at different pitch angles θ, the induced voltages in the time domain at the termination resistance of antenna is shown in Fig. 13. The induced voltages firstly increase, then decrease with the increment of the pitch angle θ. When the $\theta = 45°$, 60°, 120°, and 135°, the induced voltages reach higher values, and the peak voltage is 238 V.

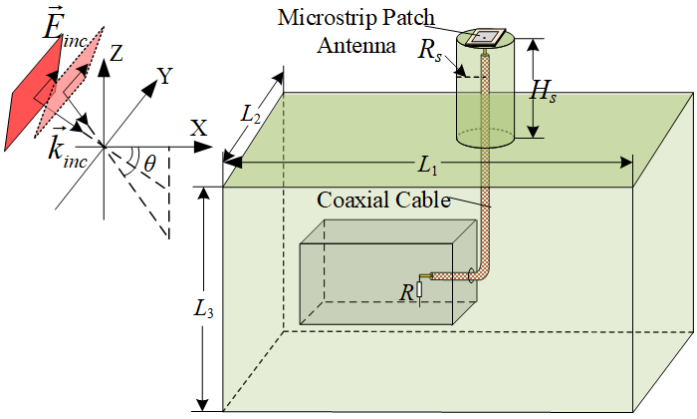

Figure 12. Considering different pitch angle θ of incident EMP.

In order to obtain the maximum value and further analyze the variation regularity of coupling response, we carried on more detailed simulations at intervals of 5° between 40° and 140° of the angles θ. Then a variation curve of peak voltage of different pitch angles could be obtained according to the simulation results shown in Fig. 13, as shown in Fig. 14. From Fig. 14, we can get that because the antenna structure is symmetrical with respect to the yoz plane, the coupling responses from 0° to 90° are completely symmetrical with those from 180° to 90°. When the angle $\theta = 50°$, the induced voltages reach the maximum values, and the peak voltage is about 254.3 V. The coupling induced voltages of pitch angles of 40° to 70° and its symmetrical angles are greater than 200 V and larger than that of other angles, which is obviously due to the fact that the angles of 40° to 70° correspond to the main lobe range of the antenna pattern. Therefore, it is relatively dangerous for the terminal electronic equipment of antenna when the antenna is illuminated by an EMP from this range of the pitch angles.

3.3. Coupling Responses Considering Different Azimuth Angle of Incident EMP

In this section, the incident EMP wave is set in the direction of $\theta = 45°$, and azimuth angle φ varies from 0° to 180° by 15° increments. Then, the induced peak voltages of the antenna at different azimuth angles are calculated, and the variation curve of peak voltage is shown in Fig. 15. From Fig. 15, we can see that the induced voltages firstly decrease, then increase with the increment of the azimuth angles φ. Obviously, the peak voltages are also symmetrical about the yoz plane.

When $\varphi = 90°$, the induced peak voltage of the antenna is approximately 0 V. This is because the electric field direction E_{inc} of EMP wave is perpendicular to the polarization direction of the antenna,

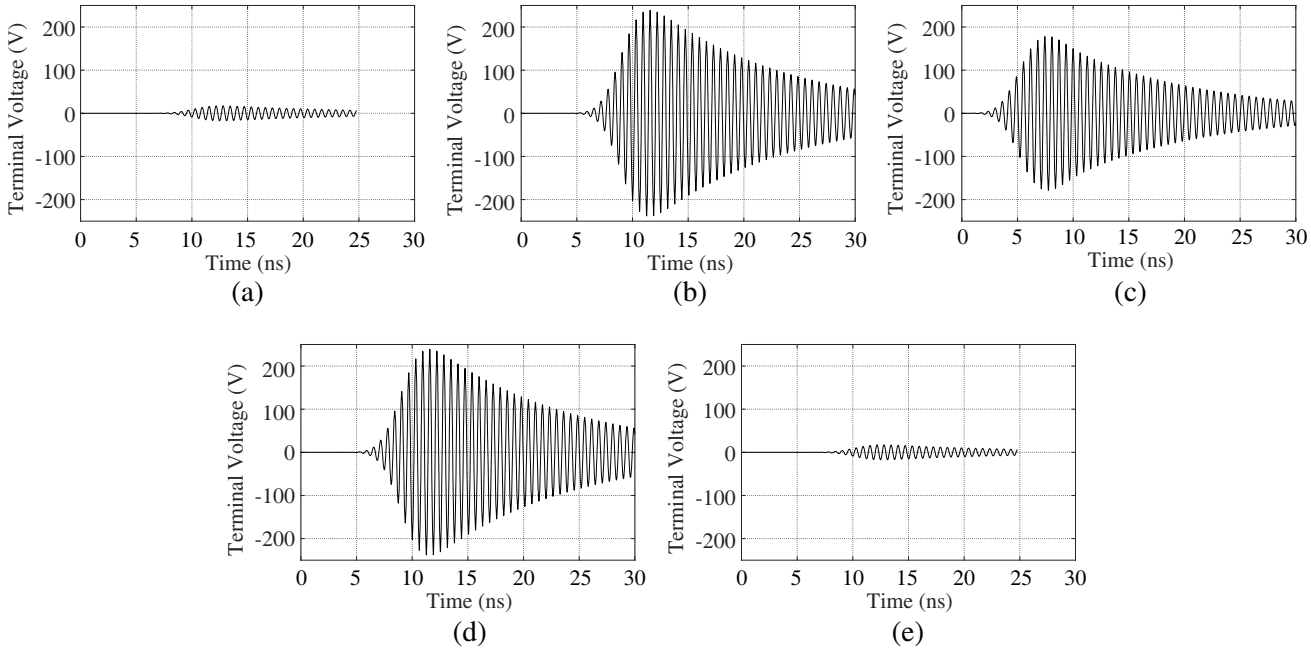

Figure 13. Induced voltage waveforms of the antenna at the thirteen pitch angles. (a) 0°, (b) 45°, (c) 90°, (d) 135°, (e) 180°.

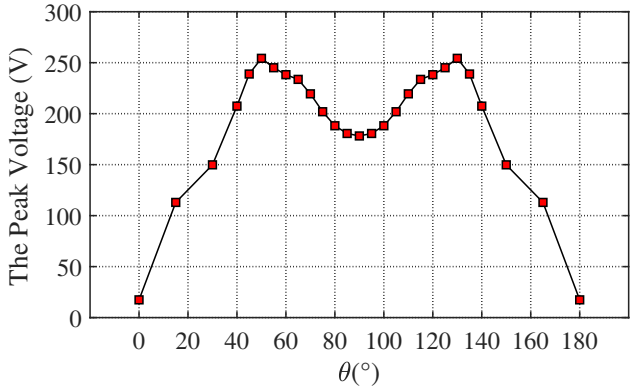

Figure 14. The variation curve of peak voltage at different pitch angles θ.

i.e., the polarization direction of EMP and antenna do not match each other. According to Figs. 14 and 15, we can get that when the EMP wave is incident in the directions of $\varphi = 0°$ and $\theta = 40°$–$70°$ and the symmetrical angles about the yoz plane, the coupling induced voltage would reach higher values, which may cause disturbance or even damage to the radio frequency (RF) receiving circuit of the antenna. Therefore, in the subsequent analysis, we would only discuss the case when the angle φ is $0°$.

3.4. Coupling Responses Considering Different Heights of the Support Structure

The influence of different heights of the support structure on the antenna coupling responses is discussed in this section. Considering the practical variable range of the support structure of the antenna, the heights H_s of the support structure are set to 0.1, 0.2, 0.3, 0.4, and 0.5 m, respectively, and then the induced peak voltages of the antenna at different pitch angles θ are calculated and shown in Fig. 16. Since the peak voltages are symmetrical about the yoz plane, we would only discuss the simulation results from 0° to 90° in the subsequent analysis. From Fig. 16, we can see that when the height of the

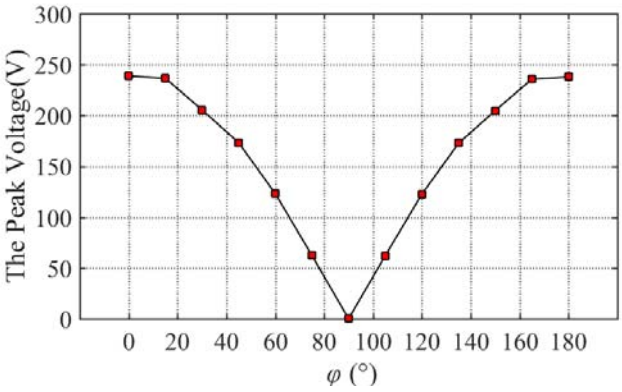

Figure 15. The variation curve of peak voltage at different azimuth angles φ.

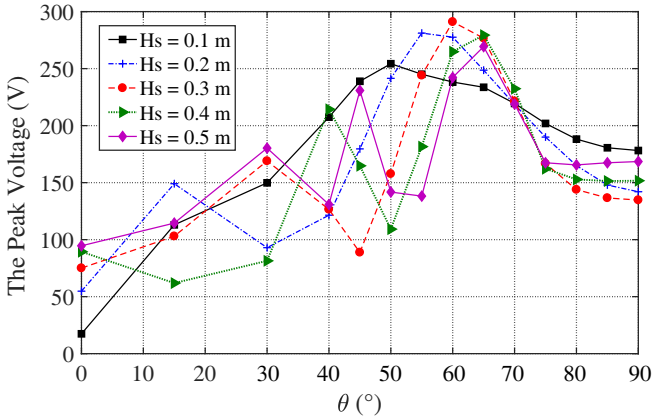

Figure 16. The variation curve of peak voltage at different pitch angles θ of different support heights.

support of the antenna changes, the induced voltage curve fluctuates with the pitch angles θ greatly. Obviously, with the increase of the height of the support structure, the characteristics of the antenna pattern become more and more complex.

According to Figs. 16, we can get that when the support is 0.1, 0.2, 0.3, 0.4, and 0.5 m high, the maximum induced voltages of the antenna are 254.3, 281.2, 291, 279.4, and 269.3 V, respectively, and the corresponding pitch angles are 50°, 55°, 60°, 65°, and 65°, respectively. When the height of the support structure is 0.3 m, the induced voltage reaches its maximum value 291 V. The difference between the maximum and minimum peak voltage is only 12%, which indicates that the support height has little effect on the maximum peak voltage. Through further analysis, we find that there are 8, 5, 4, 4, and 4 points whose peak voltages are greater than 200 V on each curve. It can be seen that the angle range of high peak voltage are gradually decreased with the increase of heights H_s. Therefore, we can get that as the heights of the support structure increase, the widths of the main lobe of the antenna pattern decrease gradually. When the heights H_s vary from 0.1 m to 0.5 m, the maximum values of induced voltage on each curve would appear near the pitch angle 60°. It can be known that no matter how high the support structure is (within the range of 0.1 m to 0.5 m), the EMP wave illuminated at $\theta = 60°$ will cause more serious coupling effects to the antenna.

3.5. Coupling Responses Considering Different Top Areas of Support Structure

After that, the influence of different top areas of the support structure on the antenna coupling responses is analyzed. The top area is determined by the radius R_s of the support structure. Similarly, according to the practical variable range of the support structure of the antenna, the radii R_s are set to 20, 40, 60,

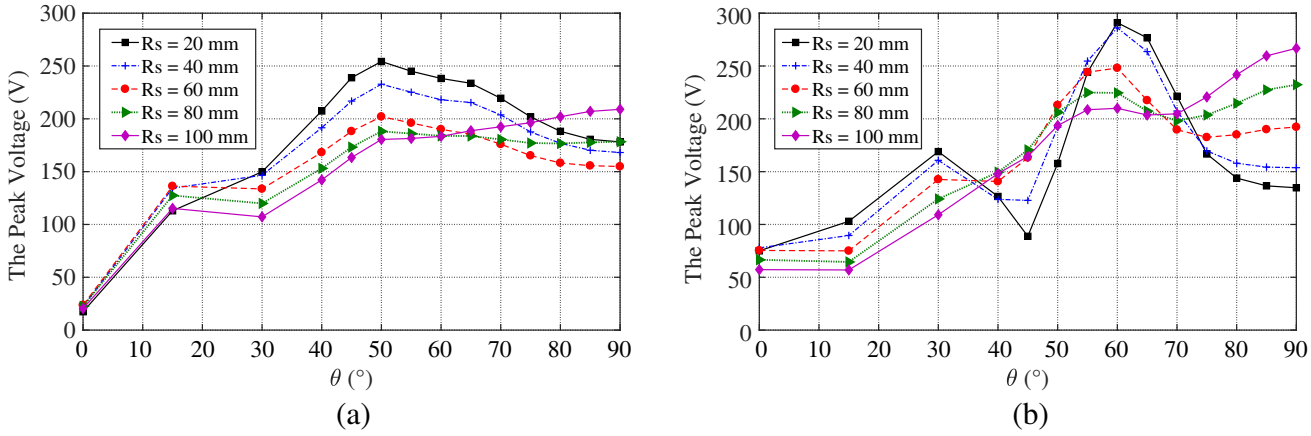

Figure 17. The variation curves of peak voltage at different pitch angles of different support radii with different heights H_s. (a) Peak voltages when the height of the support structure is 0.1 m. (b) Peak voltages when the height of the support structure is 0.3 m.

80, and 100 mm, respectively, and the heights H_s is 0.1 m and 0.3 m, respectively. Then the coupling responses of the antenna at different pitch angles are calculated. Combining the calculated results of the previous section (when the height $H_s = 0.3$ m and the radius $R_s = 20$ mm), the comparison of the variation curves of different radii R_s is shown in Fig. 17. From Figs. 17(a) and (b), we can get that as the radii R_s increase, the curves become smoother and nearly monotonically increasing at the pitch angles. When the radius R_s is greater than 80 mm, the maximum peak voltages would appear at 90° rather than 50° or 60°. According to Fig. 17, it can be found that the top areas of the support structure would change the angles at which the maximum voltages occur. Obviously, the heights of the support structure change the width of the main lobe of the antenna pattern, while the top areas would have a greater impact on the orientation of the main lobe of the antenna pattern.

3.6. Coupling Responses Considering Different Positions of Support Structure

In the above analysis, the support structure is placed at the center of the vehicle. In this section, the support structure is translated from the center of the vehicle to position 2 and 3 along the x axis and y axis, respectively, both of which are 0.1 m away from the vehicle boundary, as shown in Fig. 18. The R_s and H_s are 20 mm and 0.1 m, respectively. Then the coupling responses at different pitch angles are calculated, and the comparison of different positions is shown in Fig. 19.

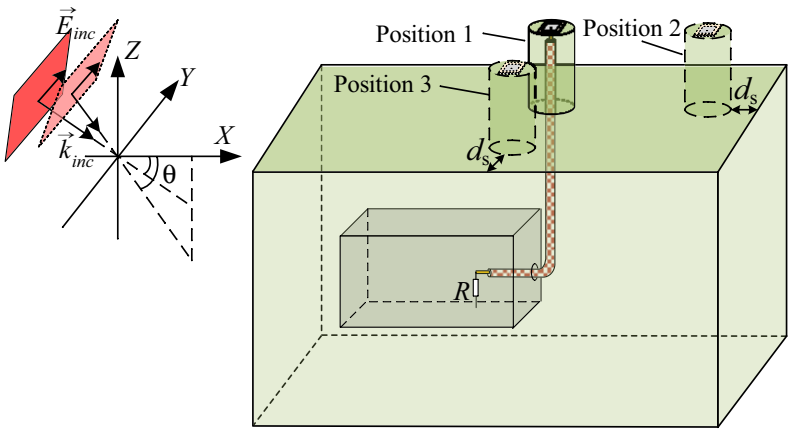

Figure 18. Considering different positions of support structure.

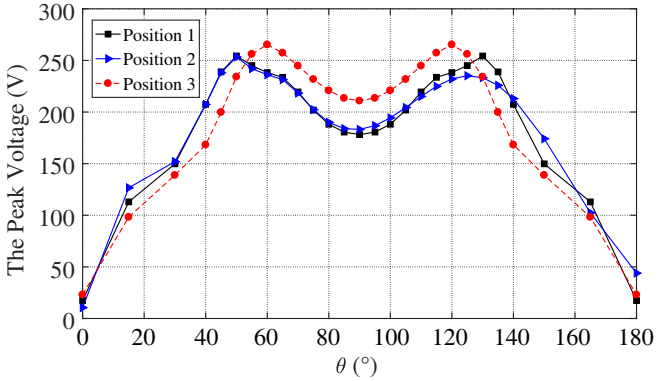

Figure 19. Comparison of the peak voltage of different support positions.

According to the simulation results, we can see that the peak voltage curve of position 1 basically coincides with the curve of position 2, while the peak voltage curve of position 3 has great difference from other two positions. When the antenna is placed at position 2, the variation curve of peak voltage is not symmetrical with respect to yoz plane, due to the different reflective areas of the antenna along the x-axis direction. The peak voltages of position 1 and position 2 in the range of 0°–90° are almost the same, while there are slight differences in the range of 90°–180°. Especially when θ is 130°, and the peak voltage of position 2 is 234.1 V, which is about 20 V lower than that of position 1. However, the peak voltages of position 3 is about 30 V larger than that of other two positions at each angle in the range of 60°–120°. Obviously, it can be concluded that the change of the position along the polarization direction of antenna has greater effects on the coupled induced voltages than that perpendicular to the polarization direction of antenna.

4. CONCLUSION

In this paper, we have proposed a hybrid FDTD method for investigating the coupling responses of the microstrip patch antenna mounted on the vehicle platform. By integrating the non-uniform mesh FDTD, thin wire model, and transmission line equation effectively, the proposed method can rapidly capture the terminal response of the antenna. Based on our hybrid method, we have analyzed the influence of different incident EMPs, different heights of the support structure, and different top areas of support structure on the coupling effects of the antenna.

From the results of calculation and analysis, it can be seen that in general, the induced voltages caused by the incident EMP with the pitch angles θ of 40°–70° and the azimuth angles φ of 0° are larger than that from other angles. When $\varphi = 90°$, the induced peak voltage of the antenna is approximately 0 V because the polarization directions of EMP and antenna do not match each other. When the height H_s of the support structure is 0.3 m, the induced voltage reaches its maximum value 291 V. No matter how high the support structure is (within the range of 0.1 m to 0.5 m), the EMP wave illuminated at $\theta = 60°$ will still cause more serious coupling effects to the antenna. When the radius R_s is greater than 80 mm, the maximum peak voltages would appear at 90° rather than 60°. Comparing the simulation results of different antenna positions, it can be concluded that the change of the position along the polarization direction of antenna has greater effects on the coupled induced voltages than that perpendicular to the polarization direction of antenna. The above simulation analysis can provide sufficient information for the design of installation structure of antenna and further electromagnetic protection of the radio frequency (RF) receiving circuit of the antenna.

ACKNOWLEDGMENT

This work was supported by the National Key Basic Research Program of China (Grant No. 2015CB857103).

REFERENCES

1. Sieger, G. E., J. H. Yee, and D. J. Mayhall, "Computer simulation of nonlinear coupling of high-power microwaves with slots," *IEEE Trans. Plasma Sci.*, Vol. 17, No. 4, 616–621, 1989.
2. Wang, J. G., Y. S. Chen, R. Y. Fan, H. Q. Yu, and D. B. Ge, "Numerical studies on nonlinear coupling of high-power microwave pulses into a cylindrical cavity," *IEEE Trans. Plasma Sci.*, Vol. 24, No. 1, 193–197, 1996.
3. Hwang, S.-M., J.-I. Hong, and C.-S. Huh, "Characterization of the susceptibility of integrated circuits with induction caused by high power microwaves," *Progress In Electromagnetics Research*, Vol. 81, 61–72, 2008.
4. You, J. W., J. F. Zhang, W. H. Gu, W. Z. Cui, and T. J. Cui, "Numerical analysis of passive intermodulation arisen from nonlinear contacts in HPMW devices," *IEEE Trans. Electromagn. Compat.*, Vol. 60, No. 5, 1470–1480, 2018.
5. Lertsirimit, C., D. R. Jackson, and D. R. Wilton, "An efficient hybrid method for calculating the EMC coupling to a device on a printed circuit board inside a cavity by a wire penetrating an aperture," *Electromagnetics*, Vol. 25, Nos. 7–8, 637–654, 2005.
6. Xie, H. Y., J. G. Wang, R. Y. Fan, and Y. N. Liu, "A hybrid FDTD-SPICE method for transmission lines excited by a nonuniform incident wave," *IEEE Trans. Electromagn. Compat.*, Vol. 51, No. 3, 811–817, 2009.
7. Xie, H. Y., J. G. Wang, Y. Li, and H. F. Xia, "Efficient evaluation of multiconductor transmission lines with random translation over ground under a plane wave," *IEEE Trans. Electromagn. Compat.*, Vol. 56, No. 6, 1623–1629, 2014.
8. Xie, H. Y., Y. Li, H. L. Qiao, and J. G. Wang, "Empirical formula of effective coupling length for transmission lines illuminated by E1 HEMP," *IEEE Trans. Electromagn. Compat.*, Vol. 58, No. 2, 581–587, 2016.
9. Ye, Z., X.-Z. Xiong, C. Liao, and Y. Li, "A hybrid method for electromagnetic coupling problems of transmission lines in cavity based on FDTD method and transmission line equation," *Progress In Electromagnetics Research M*, Vol. 42, 85–93, 2015.
10. Ye, Z. H., C. Liao, X. Z. Xiong, and M. Zhang, "The research and application of a novel time domain hybrid method for EMI analysis of a shielded device with lumped circuit," *IEEE Trans. Electromagn. Compat.*, Vol. 58, No. 4, 964–970, 2016.
11. Ye, Z. H., C. Liao, X. Z. Xiong, and M. Zhang, "A hybrid method combining the novel TD-SC technique and FDTD method for the EMI analysis of transmission line network," *IEEE Trans. Electromagn. Compat.*, Vol. 59, No. 4, 1211–1217, 2017.
12. Elshiekh, H. A., et al., "Transient response of dipole antenna using SEM-FDTD method," *Proc. 22th Nat. Radio Sci. Conf.*, 55–76, 2005.
13. Liu, Q. F., et al., "Wideband pulse response of monopole antenna under impact of an EMP," *Proc. IEEE Int. Symp. Microw., Antennas, Propag. EMC Technol. Wirel. Commun.*, 136–139, 2011.
14. Zhang, Q., J. Wang, and W.-Y. Yin, "Transient electromagnetic response of a coaxial feeding monopole antenna mounted on a rectangular metallic enclosure illuminated by electromagnetic pulses (EMP)," *PIERS Proceedings*, 1124–1128, Kuala Lumpur, Malaysia, March 27–30, 2012.
15. Liu, Q. F., X. N. Zhao, and J. W. Liu, "Transient response analysis of the monopole antenna illuminated by an external EMP source," *Proc. IEEE Int. Symp. Microw., Antennas, Propag. EMC Technol. Wirel. Commun.*, 333–337, 2013.
16. Liu, Q. F., W. Y. Yin, M. F. Xue, J. F. Mao, and Q. H. Liu, "Shielding characterization of metallic enclosures with multiple slots and a thin-wire antenna loaded: Multiple oblique EMP incidences with arbitrary polarizations," *IEEE Trans. Electromagn. Compat.*, Vol. 51, No. 2, 284–292, 2009.
17. Liu, Q. F., W. Y. Yin, J. F. Mao, and Z. Z. Chen, "Accurate characterization of shielding effectiveness of metallic enclosures with thin wires and thin slots," *IEEE Trans. Electromagn. Compat.*, Vol. 51, No. 2, 293–300, 2009.

18. Han, X., J. Wang, and Y.-S. Xia, "A novel field-line-circuit hybrid algorithm for transient responses prediction of transmission lines based on FDTD method," *Progress In Electromagnetics Research M*, Vol. 54, 163–173, 2017.
19. Wang, J., X. Han, K. Yang, and Y. S. Xia, "Hybrid FDTD method for studying electromagnetic coupling effects of transmission line networks," *IEEE Trans. Electromagn. Compat.*, Vol. 59, No. 5, 1650–1653, 2017.
20. Seaux, J. P., A. Reineix, B. Jecko, and J. H. Hamelin, "Transient analysis of a space-borne microstrip patch antenna illuminated by an electromagnetic pulse," *IEEE Trans. Electromagn. Compat.*, Vol. 33, No. 3, 224–233, 1991.
21. Taflove, A. and S. C. Hagness, *Computational Electrodynamics: The Finite-Difference Time-Domain Method*, Artech House, Norwood, MA, 2005.
22. Jiang, H. L. and H. Arai, "Analysis of computation error in antenna's simulation by using non-uniform mesh FDTD," *IEICE Trans. Commun.*, Vol. E83-B, No. 7, 1544–1552, 2000.
23. Maloney, J. G., K. L. Shlager, and G. S. Smith, "A simple FDTD model for transient excitation of antennas by transmission lines," *IEEE Trans. Antennas Propag.*, Vol. 42, No. 2, 289–292, 1994.
24. Cao, X., K. M. Luk, and C. Liang, "Analysis of a cylindrical patch antenna fed with coaxial probe using FDTD," *Microw. Opt. Techn. Lett.*, Vol. 37, No. 6, 406–408, 2003.
25. MäKinen, R. M., V. Kangas, J. Lahtinen, and M. Kivikoski, "A coaxial probe feed model for FDTD," *Microw. Opt. Techn. Lett.*, Vol. 34, No. 3, 193–198, 2002.
26. Tatematsu, A., "A technique for representing coaxial cables for FDTD based surge simulations," *IEEE Trans. Electromagn. Compat.*, Vol. 57, No. 3, 488–495, 2015.
27. Umashankar, K. R., A. Taflov, and B. Beker, "Calculation and experimental validation of induced currents on coupled wires in an arbitrary shaped cavity," *IEEE Trans. Antennas Propag.*, Vol. 35, No. 11, 1248–1257, 1987.
28. Noda, T., and S. Yokoyama, "Thin wire representation in finite difference time domain surge simulation," *IEEE Trans. Power Del.*, Vol. 17, No. 3, 840–847, 2002.
29. MäKinen, R. M., J. S. Juntunen, and M. A. Kivikoski, "An improved thin-wire model for FDTD," *IEEE Trans. Microw. Theory Tech.*, Vol. 50, No. 5, 1245–1255, 2002.
30. Railton, C. J., D. F. Paul, I. J. Craddock, and G. S. Hilton, "The treatment of geometrically small structures in FDTD by the modification of assigned material parameters," *IEEE Trans. Antennas Propag.*, Vol. 53, No. 12, 4129–4136, 2005.
31. Railton, C. J., D. L. Paul, and S. Dumanli, "The treatment of thin wire and coaxial structures in lossless and lossy media in FDTD by the modification of assigned material parameters," *IEEE Trans. Electromagn. Compat.*, Vol. 48, No. 4, 654–660, 2006.
32. Taniguchi, Y., Y. Baba, N. Nagaoka, and A. Ametani, "An improved thin wire representation for FDTD computations," *IEEE Trans. Antennas Propag.*, Vol. 56, No. 10, 3248–3252, 2008.
33. Roden, J. A. and S. D. Gedney, "Convolution PML (CPML): An efficient FDTD implementation of the CFS-PML for arbitrary media," *Microw. Opt. Techn. Lett.*, Vol. 27, No. 5, 334–339, 2000.